Comparative measurement of in plane strain by shearography and electronic speckle pattern interferometry

A. Martínez[a], J.A. Rayas[a], R. Cordero[b], and F. Labbe[c]
[a]*Centro de Investigaciones en Óptica,*
Loma del Bosque 115, Col. Lomas del Campestre, León, Guanajuato México,
Tel. (477) 4414200; Fax (477) 4414209
e-mail: amalia@cio.mx; jrayas@cio.mx
[b]*Universidad de Santiago de Chile,*
Ave. Bernardo O'higgins 3363, Santiago, Chile,
e-mail: raul.cordero@usach.cl
[c]*Universidad Técnica Federico Santa María,*
Ave. España 1680, Valparaíso, Chile
e-mail: fernando.labbe@usm.cl

Recibido el 15 de junio de 2011; aceptado el 19 de octubre de 2011

In this work, an optical setup that gives the possibility of using either ESPI or ESPSI has been implemented to assess in-plane strains induced on a composite sample. First, in-plane ESPI was used to measure displacement fields, which later allowed us to evaluate the corresponding strain fields. Next, we applied ESPSI to measure the derivative of in-plane surface displacements (the strains). The experimental results obtained by applying both techniques (ESPI and ESPSI) were compared. We found that the difference between the strain fields obtained by ESPSI and ESPI was roughly a constant. This result was expected since, although ESPI allows computing absolute strain values, the strains measured by ESPSI are relative to a reference that must be measured using an additional method. Once calibrated the system ESPSI, the ESPI could no longer be used. The strain field obtained in ESPSI is corrected by the sum of constant value calculated.

Keywords: Electronic speckle pattern interferometry; shearography; strain.

PACS: 06.20.-f; 07.60.Ly; 06.60 Mr; 06.90.+v

1. Introduction

Over recent decades, many new composites have been developed, some with very valuable properties. By carefully choosing the reinforcement, the matrix and the manufacturing process that brings them together, engineers can tailor the properties of the material to meet specific requirements. They can, for example, make the composite sheet very strong in one direction by aligning the fibers that way, but weaker in another direction where strength is not so important. They can also select properties such as resistance to heat, chemicals and weathering by choosing an appropriate matrix material. The greatest advantage of composite materials is strength and stiffness combined with lightness.

The demand for higher quality and structural reliability calls for better techniques for nondestructive evaluation of stresses in a structure. Optical methods such as Electronic Speckle Pattern Shearing Interferometry (ESPSI, also known as shearography) [1] and electronic speckle pattern interferometry (ESPI) [2] are of considerable interest because of their full-field and noncontact features. Among them, ESPSI allows direct measurement of surface displacement derivatives, and is a practical method that has received wide industrial acceptance for nondestructive testing.

Electronic Speckle Pattern Shearing Interferometry is very similar to electronic speckle pattern interferometry, and it is typically used for nondestructive testing in material analysis and strain measurement [3]. The shearography method is less susceptible to environmental noise, and operating the equipment typically requires less technical understanding. It is generally used qualitatively because additional information and processing are required to determine the absolute value of the deformation.

This technique has been extended to measure larger displacement values [4] (about 216 μm), and also used to study periodically induced deformations [5].

ESPSI can be divided into out-of-plane displacement gradient measurement and in-plane displacement gradient measurement. A combination of system ESPI and ESPSI to out-of-plane displacement gradient measurement has been implemented but the values found from both techniques have not been compared [6-8].

The determination of the reference value (constant) was measurement too by using a square grid printed by serigraphy over the illuminated surface of the specimen [3].

This work describes the above mentioned inspection techniques and examines the strain map results obtained from phase stepped ESPSI and ESPI techniques applied to composite material samples that had a hole in the sample center. In particular, the results from the ESPSI are compared with the reference ESPI results to determine how well they correlate, which ultimately attempts to determine the suitability of the ESPSI technique as an alternative ESPI inspection technique. By applying appropriate phase stepping techniques

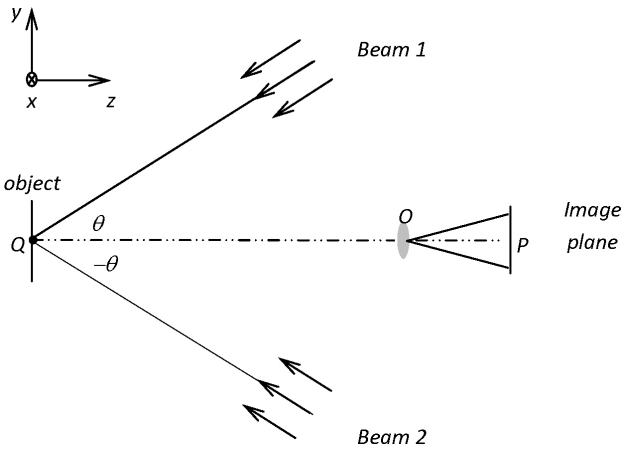

FIGURE 1. Arrangement of ESPI interferometer to measure displacement in the direction of the y-axis.

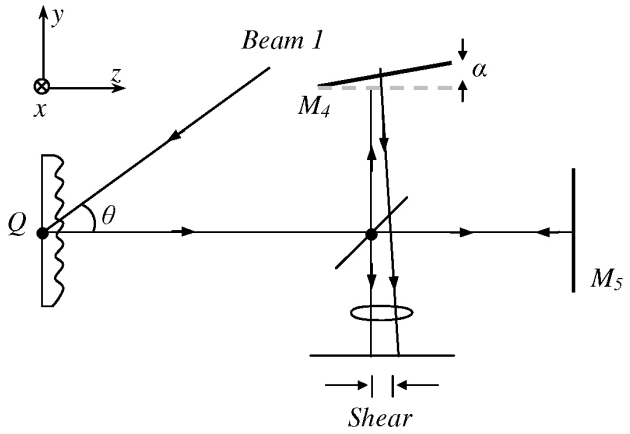

FIGURE 2. Principle of digital speckle shearography, a schematic setup.

during the process, followed by suitable phase unwrapping algorithms and reconstruction processes, captured fringe patterns can be reconstructed to represent quantifiable whole field surface strain.

2. Theory

2.1. Electronic speckle pattern interferometry

In ESPI, a speckle pattern is formed by illuminating the surface of the test object with two collimated wave fronts formed by an interferometer which has laser light as its source. A schematic of the system is shown in Fig. 1. Wave fronts 1 and 2 are symmetrically inclined at an angle θ to the surface normal to the test object on the *yz-plane*. The unloaded test object is imaged by a CCD video camera directed along the *z-axis* and on the plane of the collimated wave fronts. These wave fronts are scattered at the surface of the object and form two separate speckle patterns that interfere on the film plane of the CCD camera. The CCD camera captures this interference pattern, which is then processed by the ESPI test software and is stored as a reference pattern on the computer. When the object is subsequently loaded, the test area undergoes deformation and the collimated wave fronts are again scattered, resulting in a change in the speckle patterns. This, in turn, causes a change in the interference pattern, which is again imaged on the faceplate of the CCD camera and stored in memory. The ESPI test software is then used to process the two stored interference patterns so as to display the resulting interferogram of alternate light and dark fringes on a video monitor. The interferogram is representative of the displacement of the test object. Then the displacement field is given by [9]:

$$v\left(x,y\right)=\varphi\left(x,y\right)\frac{\lambda}{4\pi\,\sin\theta}\quad , \tag{1}$$

where λ is the wavelength of the laser light, θ the angle of inclination of the coherent wave front with respect to the surface normal on the *yz-plane*, and φ is the relative phase change between the two states.

2.2. Electronic Speckle Pattern Shearing Interferometry

A schematic diagram of an optical arrangement of oblique illumination and normal observation is shown in Fig. 2. A collimated beam lying on the *y-z plane* and making an angle θ with respect to the observation direction illuminates the object. A zoom video lens and a Michelson interferometric setup are used for imaging and shearing. To simplify the analysis, we assume that the illumination beam is collimated and the zoom lens is close to telecentric. In the setup, phase stepping is provided by one of the mirrors (PZM) in the Michelson interferometer. A small tilt to mirror M_4 introduces a lateral shift Δy perpendicular to the observation direction. The two laterally sheared wave fronts interfere with each other on the target of the CCD camera and produce the resultant speckle pattern

$$I\left(x,y\right)=\left|A\left(x,y\right)+A\left(x,y+\Delta y\right)\right|^{2}, \tag{2}$$

where A is the complex amplitude at the detecting plane. Hence, the acquired irradiance depends on the scattering properties of two small areas centered at $p\left(q\right)$ and $p\left(q+\Delta q\right)$ on the object, where Δq is the shear vector on the object [1]. When the object deforms, a new speckle pattern $I'(x,y)$ is acquired. If it is assumed that only small deformations are present, the phase change $\Delta\varphi_y(x,y)$ between $I(x,y)$ and $I'(x,y)$ is given by [10]

$$\Delta\varphi_{y}^{1}=\frac{2\pi}{\lambda}\left[\sin\theta\frac{\partial v}{\partial y}+\left(1+\cos\theta\right)\frac{\partial w}{\partial y}\right]\cdot\Delta y\quad , \tag{3}$$

where λ is the wavelength of the light, v is the in-plane displacement generated by the deformation, θ is the angle between the direction of illumination and the direction of observation, w is the out-of-plane displacement, and $\Delta y$is the magnitude of the shear along the y direction (Fig. 3, beam 1).

Similarly, one can write the equation of relative phase difference when laser illumination is supplied by beam 2

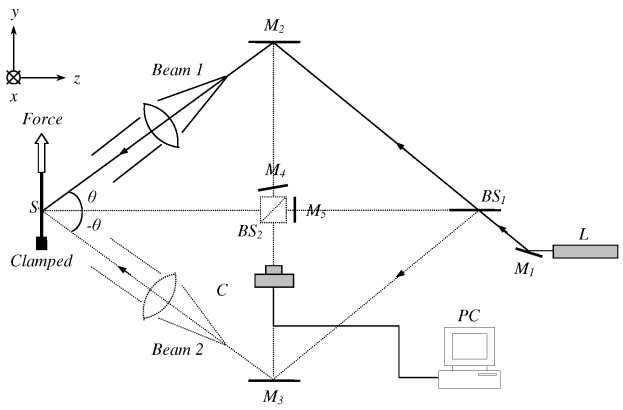

FIGURE 3. Optical setup: M_1 through M_5: mirrors; C: camera; S: specimen; BS1 and BS2: Beam splitters; L: laser; I: expanded laser beam; θ: incident angle. The pulling direction was y.

(Fig. 3). The phase change introduced by the displacement of the object is expressed by [10]:

$$\Delta\varphi_y^2 = \frac{2\pi}{\lambda}\left[-\sin\theta\frac{\partial v}{\partial y} + (1+\cos\theta)\frac{\partial w}{\partial y}\right]\cdot\Delta y \quad (4)$$

The relative phase change between the phase contours represented by Eqs. 3 and 4 is given by

$$\Delta\varphi_y^1 - \Delta\varphi_y^2 = \frac{4\pi}{\lambda}\left(\sin\ \theta\frac{\partial v}{\partial y}\right)\cdot\Delta y \quad (5)$$

3. Experimental part

A system that provides a way of combining both ESPI and ESPSI is shown in Fig. 3. The surface is illuminated by two collimated beams placed symmetrically and making an angle $\theta = 28.74°$ with respect to the surface normal. In the case of ESPI, the light path to M_4 was blocked. Using an Instron machine, a uniaxial load along the $y-$direction was applied. Each wrapped phase pattern in Fig. 4 was obtained by the digital subtraction of the phase maps measured at instants

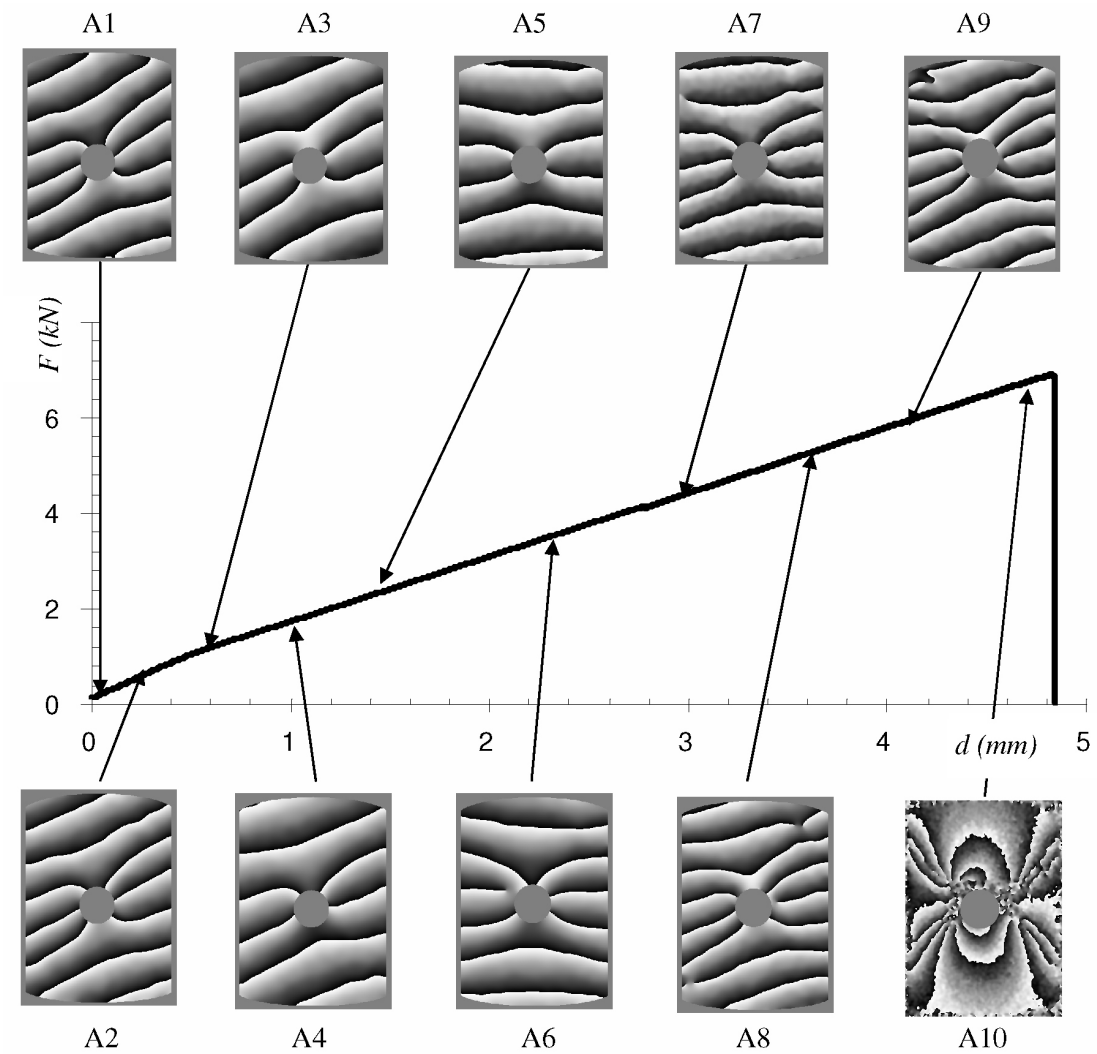

FIGURE 4. Force F–elongation d sequence of the test corresponding to sample 4. Wrapped phase patterns obtained by using an interferometer shown in figure 3. The time intervals used to generate the patterns were 30 s (patterns A1 through A9), and 5 s (pattern A10). In order to minimize the de-correlation problem due to large deformations, short time intervals were selected.

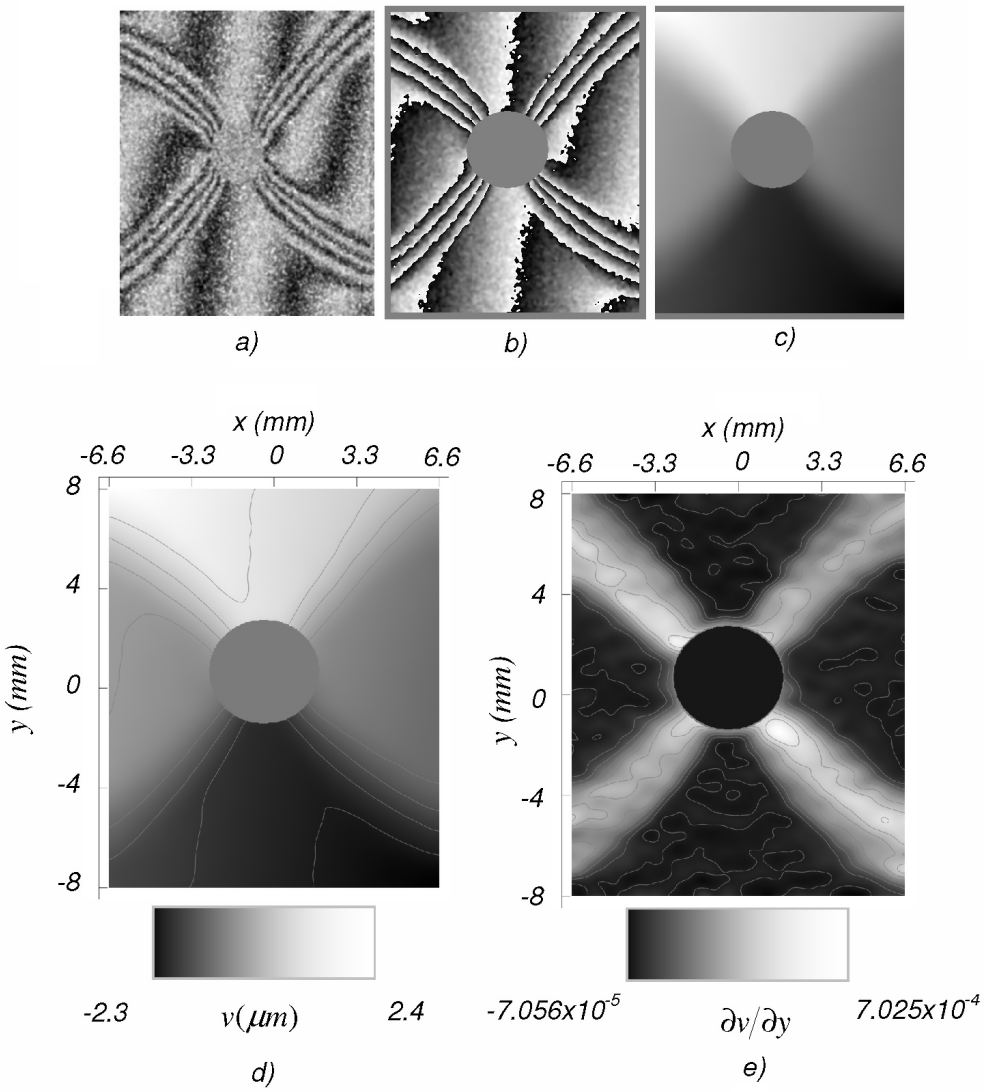

FIGURE 5. ESPI: a) Fringe pattern; b) Wrapped phase pattern; c) Unwrapped phase; d) Displacement map obtained from the unwrapped phase map shown in c); e) Strain map obtained by differentiating the displacement map shown in d) along y.

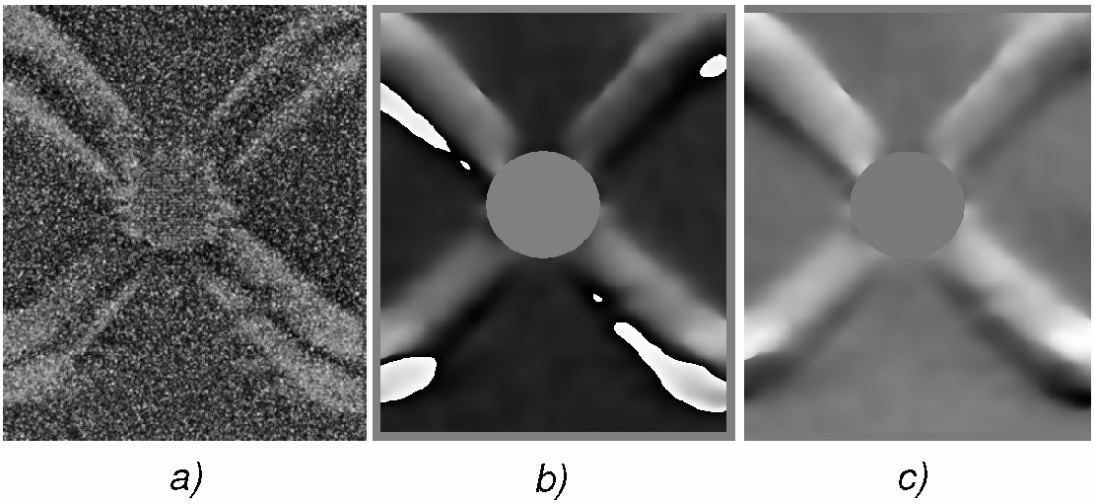

FIGURE 6. ESPSI, beam 1: a) Fringe pattern; b) Wrapped phase pattern; c) Unwrapped phase.

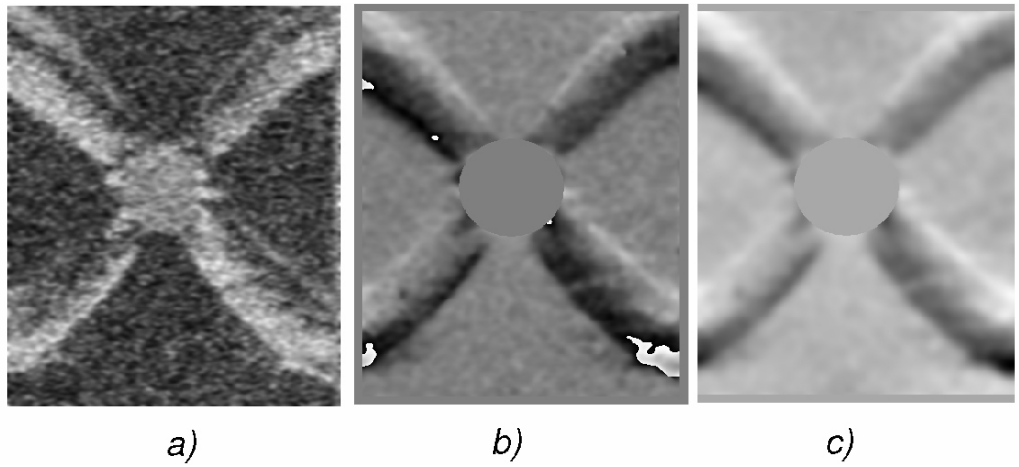

FIGURE 7. ESPSI, beam 2: a) Fringe pattern; b) Wrapped phase pattern; c) Unwrapped phase.

separated in time by an interval Δt. The first of these phase maps was measured at the load stage indicated in the plot; for example, the first phase map that allowed us to generate the wrapped phase pattern A4 was captured when sample elongation d was equal to 1 mm (see Fig. 4). The second speckle pattern was recorded 30 s later. The elongation corresponding to the second speckle pattern cannot be indicated separately in Fig. 4 because the time interval used to generate the phase pattern was relatively small (the testing machine worked at a speed of 40 μm min^{-1}). Except A10, all the other wrapped phase patterns were generated using the same time interval.

Figure 5 shows an example of data exploitation which is after A9 and before A10. To get the strain field from the displacement fields, the next evaluation step is the determination of the *displacements derivatives*. Deriving v in the y direction yields the strain (unit elongation) ε_y directly. In Fig 5e, this strain distribution is shown. The strain fields are obtained by numerical differentiation, where the length of the derivative interval Δ_y is 416 μm. It is a well known fact that noise in the data is severely amplified by differentiation. Therefore, a low-pass filter (mean filter) was applied to smooth the surfaces of Fig. 5c) before performing numerical differentiation to get the strains. The direct approach to numerical differentiation is to compute finite differences by:

$$\varepsilon_y = \frac{\partial v(x,y)}{\partial y} \approx \frac{v(x_i, y_{j+1}) - v(x_i, y_j)}{y_{j+1} - y_j}. \qquad (6)$$

The displacement maps v exhibit a circular hole at the central region of the plate (Fig. 5d)). To avoid these discontinuities across the boundary of the hole, the derivative was not calculated in the central circular region of the sample. In this case, the derivative values were substituted by derivative values obtained near to the hole's neighbourhood.

The use of ESPI and ESPSI was achieved by switching on the appropriate illumination beams. The frames relative to the deformed object state are subsequently recorded and subtracted from their corresponding initial patterns. The images resulting from ESPI and ESPSI were then digitally processed. Fringe patterns were captured by means of a CCD camera of 640×480 pixels and 8 bits. In this work, the four phase shift algorithm [2] was used to calculate the phase. Figures 6 and 7 show the experimental results rendered by the ESPSI configuration in the cases of illumination with beams 1 and 2 respectively. The fringes pattern is showed in Figs. 6a) y 7a). Figs. 6b) and 7b) show wrapped phase maps which are between values of (-π, π). These values are scaled between $(0, 255)$ gray levels to visualize like an image. The white areas correspond to high values of the wrapper (near values to π which corresponds to 255 or white area). The unwrapped phase maps were obtained by the classical technique [11] which are showed in Figs. 6c) and 7c).

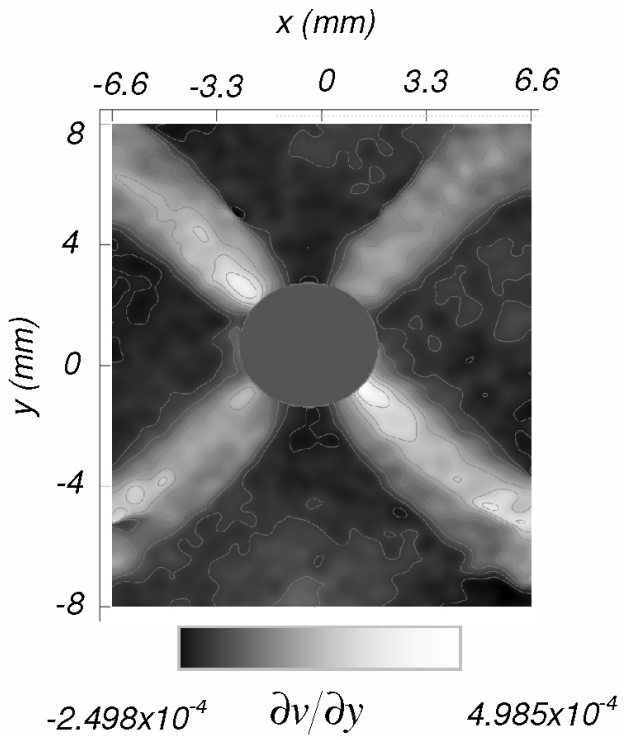

FIGURE 8. In-plane strain $\partial v/\partial y$ obtained through ESPSI.

Figure 8 shows the strain derivative distribution obtained by applying Eq. (5).

When comparing Fig. 8 and 5e), we found that the difference between the strain fields obtained by ESPSI and ESPI was roughly a constant. This result was expected since, although ESPI allows computing absolute strain values, the strains measured by ESPSI are relative to a reference that must be measured using an additional method (see [3] for details).

4. Conclusions

A stable and reliable dual-function system is proposed; it allows combining both ESPI and ESPSI into a single unit, and is an inexpensive alternative to available commercial systems. The primary advantages are the possibility of obtaining information both about an object's displacement and about its gradient as well as ESPI permits to calibrate the shearography system. From the resulting images generated by using both ESPI and ESPSI, the strain fields can be efficiently measured. In the case of ESPI, the strains are computed by differentiating the displacement fields retrieved from fringe patterns generated by interferometry when applying load to a sample; errors affecting ESPI measurements may result from both the presence of rigid body displacements resulting from excitation, and also from sensitivity to external disturbances such as vibrations. In the case of ESPSI the strains are directly retrieved from the fringe patterns, which carry information on the gradients of the relative displacement induced by the deformation of the sample; ESPSI has less sensitivity to disturbances linked to rigid body displacements and vibration, and therefore, it can be used *in situ* to detect defects in non-destructive inspections.

The experimental results obtained by applying both techniques (ESPI and ESPSI) were compared. As expected, we found that the difference between the strain fields obtained by ESPSI and ESPI was roughly a constant.

Acknowledgements

Authors wish to thank economical support from Consejo Nacional de Ciencia y Tecnología (CONACYT_Mexico). The experimental results are part of the bilateral project between Mexico-Chile: Analysis of deformation mechanisms to fruit cuticle using laser interferometry techniques. CONACYT-CONICYT project. The support of CONICYT (FONDECYT Preis 1090471, ANILLO Preis ACT98 and ANILLO Preis ACT95), UTFSM (DGIP Preis 250915) and USACH (DICYT, academic exchange program) is gratefully acknowledged.

1. W. Steinchen, L. Yang, *Digital shearography* (Bellingham, Washington USA: SPIE Press, 2003).
2. T. Kreis, *Holographic interferometry* (Bremen, Germany: Akademie Verlag 1996) 261-263 and 123-132.
3. F. Labbe, R. Cordero, A. Martínez, and R. Rodríguez-Vera, *Measurement Science Technology* **16** (2005) 1677-1683.
4. R.A. Martínez-Celorio, G.H. Kaufmann, and G. Mendiola, *Optical Engineering* **39** (2000) 751-757.
5. P.D. Ruiz, A. Dávila, G. Mendiola, G. Kaufmann, *Optical Engineering* **40** (2001) 318-324.
6. B. Bhaduri, N. Krishna Mohan, M.P. Kothiyal, and R.S. Sirohi, *Optics Express* **14** (2006) 11598-11607.
7. D. Francis, R.P. Tatam and R.M. Groves, *Measurement Science and Technology* **21** (2010) 102001.
8. P.A. Fomitchov and S. Krishnaswamy, *Measurement Science and Technology* **8** (1997) 581–583.
9. A. Martínez, R. Rodríguez-Vera, J.A. Rayas, and H.J. Puga, *Optics Communications* **223** (2003) 239-246.
10. P.K. Rastogi, *Journal of Modern Optics* **43** (1996) 1577-1581.
11. D. Malacara, M. Servín, and Z. Malacara, *Interferogram Analysis for Optical Testing* (Boca Raton, FL.: Taylor&Francis, Second Edition, 2005) pp. 493-500.